Int. J. Electrochem. Sci., 6 **(2011)** 4504 - 4513

International Journal of
ELECTROCHEMICAL
SCIENCE
www.electrochemsci.org

Rational Synthesis of Coaxial MoO_3/PTh Nanowires with Improved Electrochemical Cyclability

Shuo Li[1,#], *Chun-Hua Han*[1,#], *Li-Qiang Mai*[1, 2,*], *Jiu-Hui Han*[1], *Xu Xu*[1], *Ya-Qin Zhu*[1]

[1] State Key Laboratory of Advanced Technology for Materials Synthesis and Processing, WUT-Harvard Joint Nano Key Laboratory, Wuhan University of Technology, Wuhan, 430070, China
[2] Department of Chemistry and Chemical Biology, Harvard University, Cambridge, Massachusetts 02138, USA
[#]contributed equally to this work.

[*]E-mail: mlq@cmliris.harvard.edu

Received: 30 July 2011 / *Accepted:* 6 September 2011 / *Published:* 1 October 2011

It is of great interest to fabricate heterostructured nanowires and make full use of the synergistic effect in improving the performance of Li-ion battery electrode materials. Here we designed and demonstrated the synthesis of MoO_3/PTh coaxial nanowires via *in-situ* polymerization of thiophene monomers on the surface of hydrothermally synthesized MoO_3 nanowires. The resulting coaxial nanowires were characterized by X-ray Diffraction, Fourier Transform Infrared Spectroscopy, Field Emission Scanning Electron Microscopy, Thermogravimetric Analysis and electrochemical performance test. The results indicate the homogeneous layer of PTh is coated on the surface of MoO_3 nanowires, and the coaxial nanowires exhibit a significant enhancement of capacity retention rate from 49% of MoO_3 nanowires to 83% of MoO_3/PTh coaxial nanowires after 45 cycles. The theoretical analyses of a certain amount of capacity reduction after PTh coating are given.

Keywords: Molybdenum trioxide nanowires, Polythiophene, Coaxial nanowires, Characterizations, Electrochemistry

1. INTRODUCTION

Nanoscale materials have attracted much attention because of their interesting properties intrinsically associated with their nanoscale morphology and correlative effects such as small size effect, surface effect, quantum size effect and quantum tunnel effect. Among these, one-dimensional (1D) nanostructured materials are of both fundamental and technological interest. They not only exhibit outstanding electronic and optical properties but also act as the critical component in the potential nanoscale device applications[1-8]. To date, 1D nanostructured materials, ranging from

nanowires (NWs), nanotubes(NTs), nanorods (NRs) to nanobelts (NBs), have been introduced to applications as electrode materials in lithium-ion batteries, and have extended a new direction for improving both capacity and lifetime of these energy storage devices[9-14]. Compared with bulk materials, 1D nanostructured electrode materials have a short Li-ion insertion/extraction distance, facile strain relaxation upon electrochemical cycling, enhanced electron transport within the nanomaterials, and very large surface to volume ratio to contact with the electrolyte[15,16]. Specially, NWs, with relatively large aspect ratio, need only make a few points of contact to ensure electron transport. Many investigations have been conducted to fabricate and modify NWs to obtain superior performance[5,13,14,17-22].

Among the many materials which can be synthesized into nanostructured architectures, molybdenum oxides have long been defined as promising cathode materials with the high theoretical capacity and as attractive candidates for commercial applications[23,24]. All of these mainly result from their layered structures with the accommodating interlayer space offering efficient tunnels for lithium ion intercalation and deintercalation. Moreover, molybdenum oxides are endowed with abundant oxidation states and various coordination polyhedra, which allow the controlling of structural parameters to further improve their structure-directed properties[25]. However, molybdenum oxides have long suffered from serious capacity fading issues upon cycling due to the kinetic limitations for deep charge/discharge and limited diffusion of lithium ion in the solid state, which serves as the main challenge calling for further explorations. To overcome these problems, an effective way is to coat the pristine particles with a conductive layer.

Since Shirakawa et al. discovered that polyacetylene can reach extremely high electrical conductivities[26], the field of conducting polymers has attracted the interest of thousands of scientists. In quest of commercially viable conducting polymers, polythiophene(PTh) and its derivatives have always been one of the most promising candidates motivated by high environmental stability, moderate band gap, low redox potential, high optical transparency in its electrically conductive state, general facility for structural modifications and controllable for electrochemical behavior[27]. Though many researches of polymer/metal oxide coaxial NWs were reported like PANI/V_2O_5[28], PPy/TiO_2[29], PEDOT/MnO_2[30] and so on, there're few reports about MoO_3/PTh coaxial NWs' synthesis and characterization. Hence we designed and demonstrated a facile method to fabricate MoO_3/PTh coaxial NWs. We focus on their cathode performance for lithium-ion batteries and simultaneously try to probe the specific interactions between the PTh and MoO_3, and how these interactions contribute to enhance the properties of the coaxial NWs. This method provides a possible polymer-coating synthesis route, which can be extended to many other materials.

2. EXPERIMENTATION

2.1. Preparation

MoO_3 NWs were synthesized via a hydrothermal synthesis technique as follows: 25 ml H_2O_2(30%) was added dropwise into 2.3985 g molybdenum powder under water-cooling condition until the clear orange peroxomolybdic acid sol was obtained, then the sol was agitated rapidly for 4h

before transferring into a Teflon-lined autoclave and kept at 180 °C for 4 h. The autoclave was left to cool, and the precipitate was filtered out and rinsed with deionized water for three times.

To attain the PTh-coated MoO_3 NWs, 0.1 g as-prepared MoO_3 NWs were added into 40ml chloroform, then treated by 30 min agitation and 30 min ultrasonic treatment before transferring into a flask. A certain amount of thiophene monomers (mass ratio of MoO_3:Th is 1:0.2) were added and agitated with reflocculated MoO_3 NWs for 1h to ensure complete mixing. To this mixture, a given amount of oxidizing agent (4 times of thiophene monomers in molar ratio), iron (III) chloride ($FeCl_3$, dispersed in 20 ml chloroform), was added dropwise and then kept under refluxing condition for 4h. Resultant MoO_3/PTh coaxial NWs was filtered off and washed repeatedly with ethanol and water and the dark red powder was dried at 80 °C for 8 h.

2.2. Characterization

An X-ray diffraction (XRD) measurement was performed using a D/MAX-III X-ray diffractometer (Rigaku, Japan) with graphite-mono chromatized CuKa (1.5406 Å) radiation. Fourier transformed infrared (FTIR) absorption spectra were recorded using the 60-SXB IR spectrometer. Thermogravimetric analysis (TGA) was performed using a Netzsch STA 449F3 simultaneous thermal analyzer at a heating rate of 10 °C/min in air. Field emission scanning electron microscopy (FESEM) images were collected with a Hitachi S-4800 at an acceleration voltage of 20 kV. Batteries were fabricated using a lithium pellet as the anode, 1M solution of $LiPF_6$ in ethylene carbon (EC)/dimethyl carbonate (DMC) as electrolyte, and a pellet made of the NWs, acetylene black in a 60:40 weight ratio as the cathode, with 2 drops of PTFE(polytetrafluoroethylene) as the binder. Galvanostatic charge/discharge tests were performed over the potential region of 1.5-4.0 V at a current density of 40 mA/g and temperature of 25 °C.

3. RESULTS AMD DISCUSSION

3.1 XRD Analysis

X-ray diffraction (XRD) measurement was first used to study the phase structure of the sample. Figure 1 shows the XRD patterns of MoO_3 NWs and MoO_3/PTh NWs, respectively. The XRD of MoO_3 shows the orthorhombic structure referred to JCPDS No. 89-5108, and the strong intensities of (020), (040) and (060) peaks indicate the anisotropic growth of the nanostructure[31]. The peaks of MoO_3/PTh NWs are consistent with the MoO_3 characteristic peaks with no shift occurring, indicating there's no intercalation of PTh into layers of MoO_3. This phenomenon verified our hypothesis that the PTh was coated on the surface of MoO_3 NWs. Notably, the intensities of (020), (040) and (060) peaks are much weaker for MoO_3/PTh than those of MoO_3 NWs, while the intensities of (110) and (021) have become stronger. These indicate that the preferred orientation of nanowires becomes relatively less obvious after the coating of PTh. The hydrothermally synthesized MoO_3 NWs tend to form bundles as a result of self-aggregation, while this trend turns to be weaker for MoO_3/PTh coaxial nanowires as indicated in the SEM images (Figure 2). In addition, as a result of ultrasonic treatment, magnetic stirring and thermal vibration, some nanowires will rupture during the reaction and the length

of resulting MoO_3/PTh NWs is relatively less uniform. The coating of an organic layer on MoO_3 NWs could also lead to the decreased intensities of (020), (040) and (060) peaks.

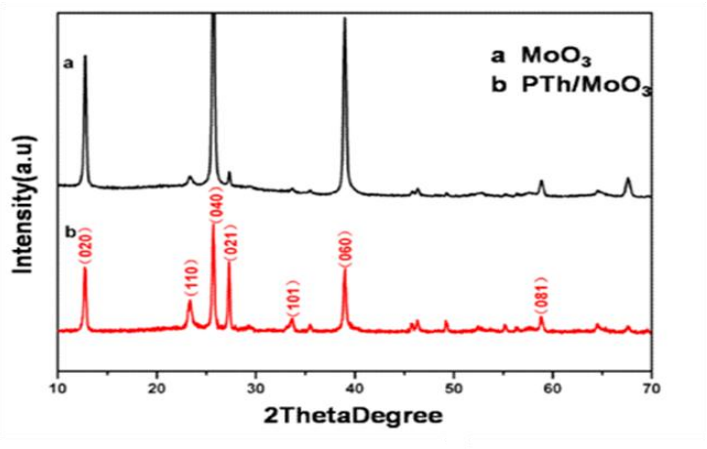

Figure 1. XRD patterns of MoO_3 NWs(a) and MoO_3/PTh coaxial NWs (b)

3.2. SEM Analysis

The morphology of as-synthesized MoO_3 NWs and MoO_3/PTh coaxial NWs were characterized by SEM. Figure 2a and 2b give the images of MoO_3 NWs, which have a diameter of 150~400nm and length of 10~20 μm, and exhibit as a template for coaxial NW synthesis. Figure 2c and 2d show the MoO_3/PTh coaxial SEM images. After the polymerization of thiophene monomers on the surface of MoO_3 NWs, the morphology of the polymer coated MoO_3 coaxial NWs are similar to that of pristine MoO_3 NWs; only the diameter is much bigger than that of corresponding MoO_3 NWs and the surface become rougher, which indicates that there are polymers coated on the surface of MoO_3 NWs. There are no PTh fragments observed in SEM images, indicating the PTh layer is homogeneously coated on MoO_3 NWs.

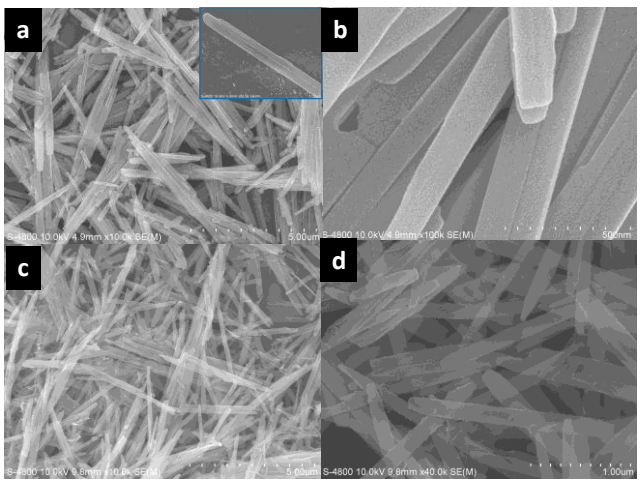

Figure 2. SEM images of MoO_3 NWs(a,b) and MoO_3/PTh coaxial NWs(c,d)

The growth mechanism of MoO_3/PTh coaxial NWs was proposed and illustrated as shown in Figure 3. During the polymer coating process, the thiophene monomers are adsorbed on the MoO_3 NWs surface due to the large specific surface area of NWs. Then the introduction of $FeCl_3$ as the oxidant leads to the *in-situ* uniform polymerization of thiophene monomers on the MoO_3 NWs.

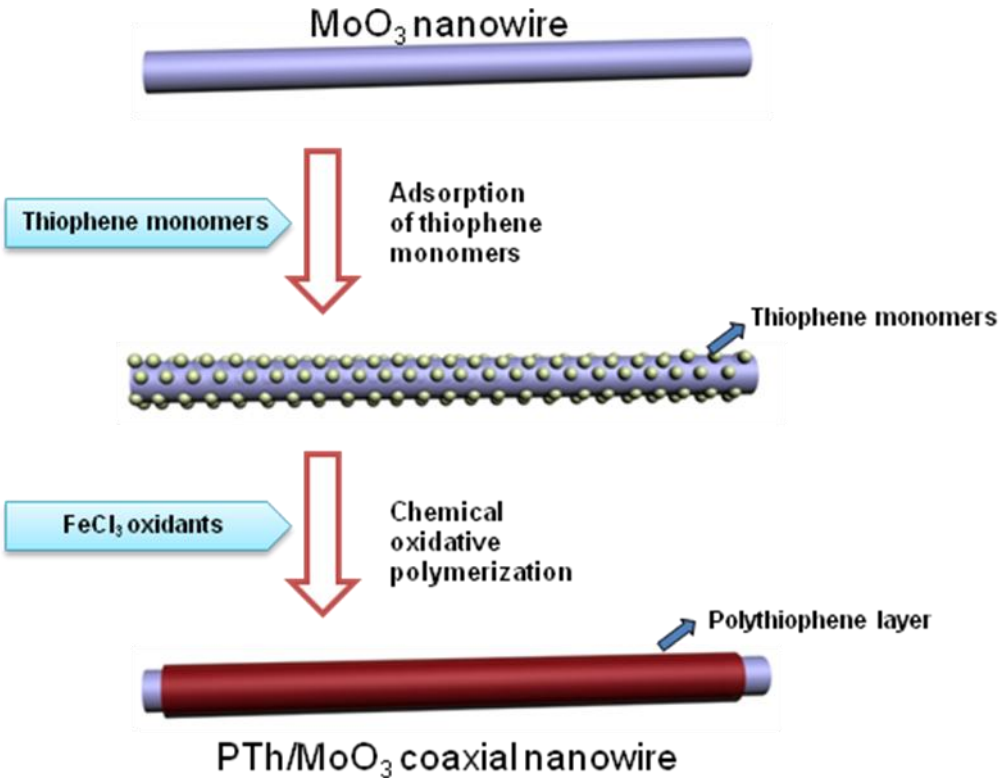

Figure 3. Synthesis processes schematic of MoO_3/PTh coaxial nanowires

3.3 FTIR Analysis

FTIR analysis was conducted to confirm the presence of PTh in the products. In Figure 4, curve a, b and c corresponds to MoO_3 NWs, MoO_3/PTh NWs and PTh, respectively. In curve 4b, peaks around 1000 cm^{-1}, 864 cm^{-1}, 554 cm^{-1} are attributed to Mo-O_1, Mo-O_2, Mo-O_3 stretching modes[32]. Vibrations around 2922cm^{-1}, 1433cm^{-1} and 1376cm^{-1} are assigned to the stretching of C-H, C=C and C-C, and peaks around 998 cm^{-1}, 697 cm^{-1} to the stretching of C-S in thiophene ring. The broad band in 3443 cm^{-1} indicates the presence of H_2O in the product. These characteristic absorption peaks indicate the products have the composition of MoO_3 and PTh. Compared with curve a and c, the peaks of curve b are slightly weaker, due to the interaction between MoO_3 and PTh. The FTIR analysis clearly indicates the existence of PTh.

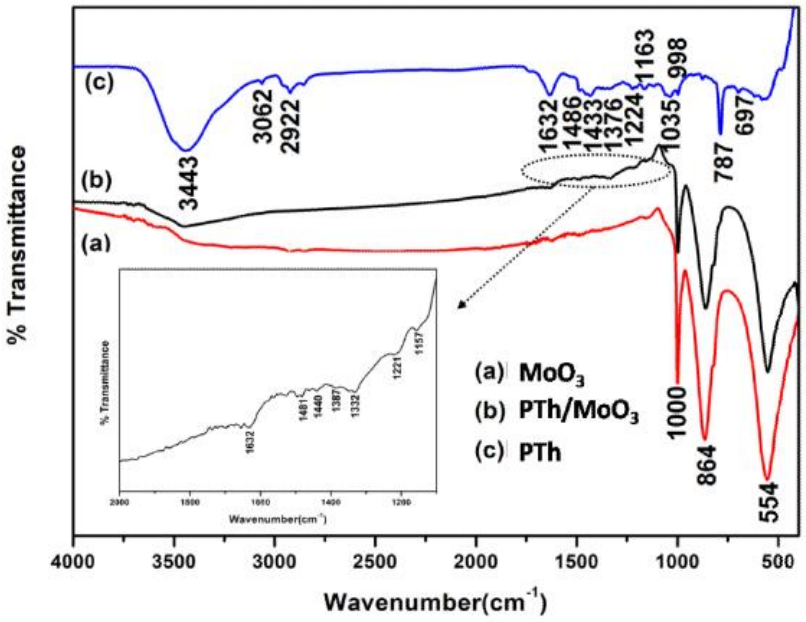

Figure 4. FTIR spectra of the MoO_3 NWs (a), MoO_3/PTh coaxial NWs (b) and PTh(c)

3.4 TGA Analysis

The thermal analysis of MoO_3/PTh coaxial NWs in air was examined by TGA experiments as shown in Figure 5.

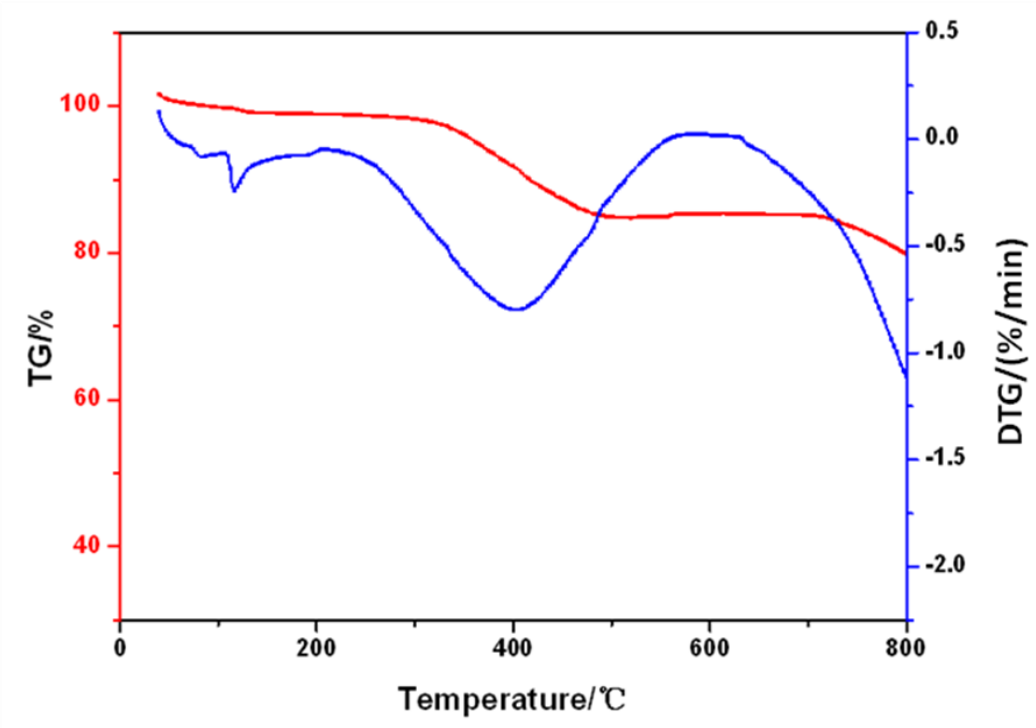

Figure 5. TG and DTA curve of the MoO_3/PTh coaxial NWs

The TG curve (red line) shows a three step decomposition of the MoO_3/PTh coaxial NWs. The first step up to 116℃ is attributed to the removal of water on the surface of the product, confirmed by the endothermic peak of the DTG curve (blue line). The weight loss at 400℃ is due to the combustion of the polymer component, which corresponds well to the exothermic DTG peak. This phenomenon proves the presence of the PTh components. When PTh was totally combusted, a mass decrease rate of 14.7% can be clearly detected. The last decrease of TG curve at 790 ℃ was attributed to the melting of the MoO_3 and followed by the sublimation. This TGA analysis further proved the successful polymerization of PTh in the products.

3.5. Electrochemical performance

Figure 6a and 6b demonstrate the potential versus capacity curves of the 3rd and 10th cycles for the pristine MoO_3 NWs and MoO_3/PTh coaxial NWs respectively, at a constant current density of 40mA/g in the voltage range between 1.5V and 4.0V. For pristine MoO_3 NWs, The 3rd discharge and charge capacities are both 213mAh/g, showing no capacity loss. The typical plateaus corresponding to the phase transitions of crystalline MoO_3 were obviously observed. After 10 cycles, the capacity drops to 176mAh/g, showing a capacity loss of 17.4%. The charge/discharge behavior still occurred, which means irreversible Li_xMoO_3 were not formed. For MoO_3/PTh coaxial NWs, the 3rd and 10th discharge capacity are 126mAh/g and 130mAh/g respectively, showing no capacity fading. The coulombic efficiency versus cycle number of MoO_3 NWs and MoO_3/PTh coaxial NWs are shown in Figure 5c. The coulombic efficiency is the fraction of the electrical charge stored during charging that is recoverable during discharge, indicating the reversible lithium ions as percentage of the total lithium ions. Both products have the coulombic efficiency above 90%, but compared with MoO_3 NWs, the coulombic efficiency of MoO_3/PTh coaxial NWs are more stable, due to the protection of PTh as the shell of NWs.

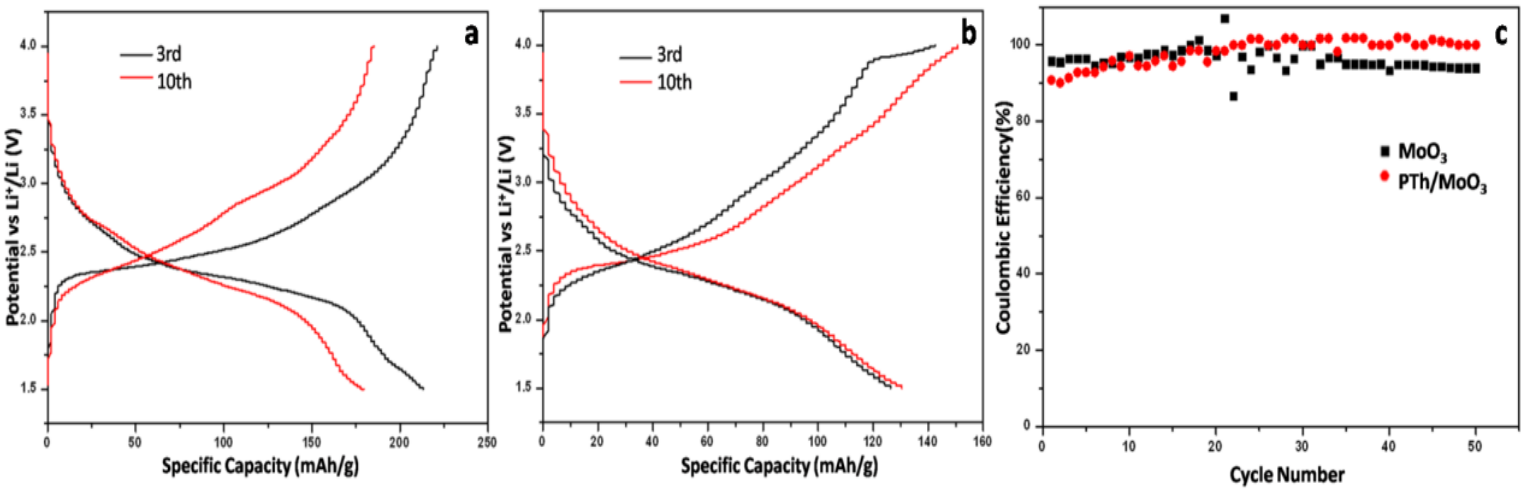

Figure 6. Potential versus Capacity curves of the 3rd and 10th cycles for the pristine MoO_3 NWs (a) and MoO_3/PTh coaxial NWs (b), and Coulombic efficiency(c)

Figure 7a depicts the comparative cycling performance of MoO_3 NWs and MoO_3/PTh coaxial NWs up to 45 cycles, respectively. At the first 20 cycles, the capacity of MoO_3 NWs exceeds the MoO_3/PTh coaxial NWs but decreases rapidly. The capacity retention of MoO_3 NWs is only 49%, while the MoO_3/PTh coaxial NWs have significantly improved capacity retention of 83% after 45 cycles. This is because during the charge-discharge cycling, lithium ions are intercalated and deintercalated into/from the electrode, which induces large strains in the MoO_3 host material and leads to volume expansion and fracture[33]. These induced structural issues cause the decrease of the lifetime of LIBs. By coating the PTh layer on the MoO_3 NWs, the structure expansion of MoO_3 is effectively restricted, thus the cycleability is improved.

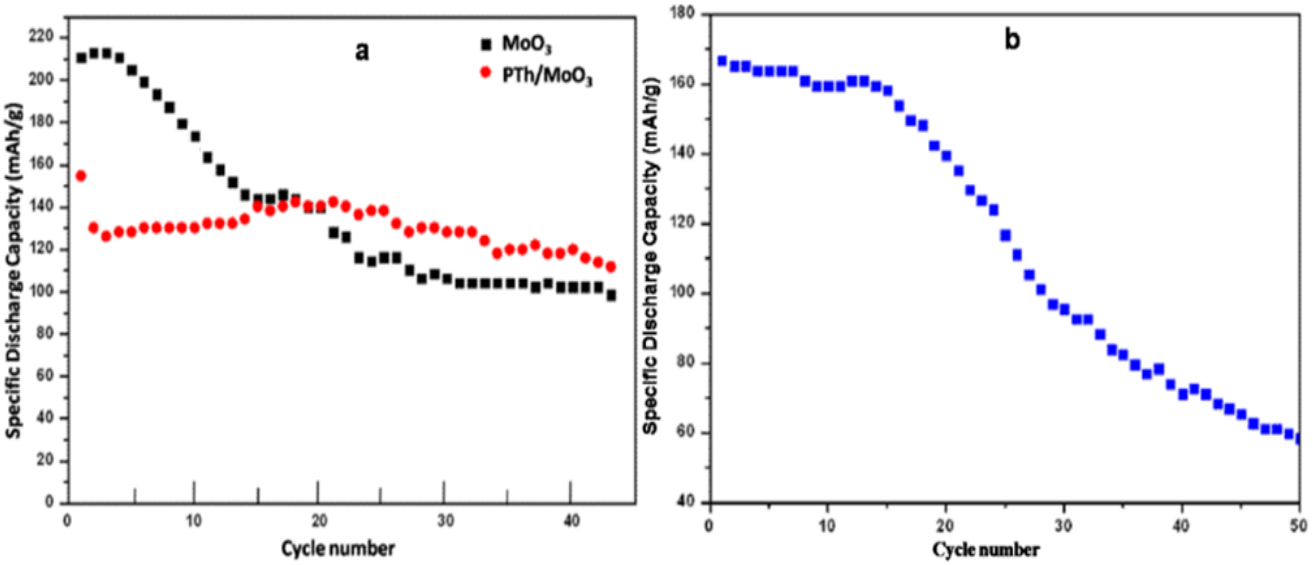

Figure 7. Cycling performance of MoO_3 NWs and MoO_3/PTh coaxial NWs(a) and simple mixed MoO_3/PTh mixture(b)

However, the initial specific capacity after PTh coating have a decrease of about 50mAh/g, this is due to the introduction of low-capacity PTh component. As reported[34], the electrochemical performance in lithium ion batteries of pure PTh synthesized via oxidation polymerization reaction is 17 mAh/g. Figure 7a indicates that the initial capacity of MoO_3 NWs is 210 mAh/g. As observed from the thermogravimetric analysis, the resulting MoO_3/PTh nanocomposites consist of 85.3% MoO_3 and 14.7% PTh (mass percent). So the approximate capacity of MoO_3/PTh composites should be:

$$C=C_{MoO3}\times 85.3\%+C_{PTh}\times 14.7\% = (210\times 85.3\%+17\times 14.7\%)\ mAh/g=181.6\ mAh/g$$

The MoO_3/PTh coaxial NWs have an initial capacity of approximately 160mAh/g (Figure 7a), which is close to the calculated value. This calculation gives a possible explanation of the inevitability of capacity loss with the introduction of low-capacity PTh component. Similar phenomenon of initial capacity decrease of metal oxide NWs after polymer coating was also reported[35]. To further prove our hypothesis we conducted a control experiment, in which MoO_3 NWs and PTh were mixed via

simple grounding (in the same amount and ratio of MoO_3/PTh coaxial NWs) and made into electrodes. Figure 7b is the cycling performance of simple mixed MoO_3/PTh. The capacity of the first cycle is 169 mAh/g, approximate to the calculated 181.6 mAh/g. However, after 50 cycles the capacity is only 58 mAh/g and the capacity retention is only 34%, much lower than that of MoO_3/PTh coaxial NWs. This indicates that coaxial MoO_3/PTh NWs improve the capacity retention greatly, only at a certain cost of inevitable capacity loss.

Polymer coating enhances the cycling stability but with a decrease in capacity in electrochemical performance analogously to prelithiation treatment in our previous work[19, 36]. However, the mechanisms are different. The reduction of discharge capacity of the lithiated MoO_3 nanobelts is probably because Li-ions had occupied some space of the interstitial sites during the hydrothermal reaction, while the capacity decrease after polymer coating results from the introduction of low-capacity component. Compared to prelithiation method, polymer coating retains the integrity of the crystal structure, thus it can be extended to many other materials.

4. CONCLUSIONS

In summary, we have developed a facile method to fabricate MoO_3/PTh coaxial NWs by coating PTh on the as-prepared MoO_3 NWs. This reaction takes place with the *in-situ* oxidation polymerization method in the presence of an external oxidizing agent. Analyses of the experiment data presented here suggest the existence of PTh on the surface of MoO_3 NWs. The electrochemical tests also indicate that the capacity retention rate is significantly enhanced from 49% for MoO_3 NWs to 83% for MoO_3/PTh coaxial NWs after 45 cycles. A theoretical calculation was given to explain the certain capacity reduction after PTh coating.

ACKNOWLEDGEMENTS
This work was supported by the National Nature Science Foundation of China (51072153, 50702039), Program for New Century Excellent Talents in University (NCET-10-0661) and the Fundamental Research Funds for the Central Universities (2010-II-016).

References

1. B. Tian, X. Zheng, T.J. Kempa, Y. Fang, N. Yu, G. Yu, J. Huang and C.M. Lieber, *Nature*. 449 (2007), 885.
2. X. Jiang, B. Tian, J. Xiang, F. Qian, G. Zheng, H. Wang, L. Mai, C. M. Lieber, *P Natl Acad Sci USA*, 108(2011), 12212.
3. W. Chen, C. Zhou, L. Mai, Y. Liu, Y. Qi and Y. Dai, *J Phys Chem C*. 112 (2008), 2262.
4. S. Xu, Y. Qin, C. Xu, Y. Wei, R. Yang and Z. Wang, *Nat Nanotechnol*. 5 (2010), 366.
5. M. Law, L.E. Greene, J.C. Johnson, R. Saykally and P. Yang, *Nat Mater*. 4 (2005), 455.
6. L. Mai, L. Xu, Q. Gao, C. Han, B. Hu and Y. Pi, *Nano Lett.* 10(2010), 2604.
7. C. Zhou, L. Mai, Y. Liu, Y. Qi, Y. Dai and W. Chen, *J Phys Chem C*. 111 (2007), 8202.
8. L. Mai, Y. Gu, C. Han, B. Hu, W. Chen, P. Zhang, L. Xu, W. Guo and Y. Dai, *Nano Lett*. **9** (2009), 826.

9. A.I. Hochbaum and P. Yang, *Chem Rev*. 110 (2009), 527.
10. L. Mai, W. Guo, B. Hu, W. Jin and W. Chen, *J Phys Chem C*. 112 (2008), 423.
11. P.L. Taberna, S. Mitra, P. Poizot, P. Simon and J.M. Tarascon, *Nat Mater*. 5 (2006), 567.
12. L. Mai, C. Lao, B. Hu, J. Zhou, Y. Qi, W. Chen, E. Gu and Z. Wang, *J Phys Chem B*. 110 (2006), 18138.
13. M.S. Park, G. Wang, Y. Kang, D. Wexler, S. Dou and H. Liu, *Angewandte Chemie*. 119 (2007), 764.
14. L. Mai, F. Yang, Y. Zhao, X. Xu, L. Xu, B. Hu, Y. Luo, H. Liu. *Mater Today*, 14(2011), 346.
15. Z. Chen, Y. Qin, D. Weng, Q. Xiao, Y. Peng, X. Wang, H. Li, F. Wei and Y. Lu, *Adv Funct Mater*. 19 (2009), 3420.
16. A.Magasinski, P. Dixon, B. Hertzberg, A. Kvit, J. Ayala and G. Yushin, *Nat Mater*. 9 (2010), 353.
17. D.W. Kim, I.S. Hwang, S.J. Kwon, H.Y. Kang, K.S. Park, Y.J. Choi, K.J. Choi and J.G. Park, *Nano Lett*. 7 (2007), 3041.
18. L. Mai, Y. Dong, L. Xu and C. Han, *Nano Lett.* 10(2010), 4273.
19. L. Mai, B. Hu, W. Chen, Y. Qi, C. Lao, R. Yang, Y. Dai and Z. Wang, *Adv Mater*. 19 (2007), 3712.
20. L. Mai, L. Xu, C. Han, X. Xu, Y. Luo, S. Zhao and Y. Zhao, *Nano Lett*. 10(2010), 4750.
21. W. Zhou, C. Cheng, J. Liu, Y.Y. Tay, J. Jiang, X. Jia, J. Zhang, H. Gong, H.H. Hng and T. Yu, *Adv Funct Mater*. 21(2011), 2349.
22. L. Mai, F. Yang, Y. Zhao, X. Xu, L. Xu and Y. Luo, *Nat Commun*. 2 (2011), 381.
23. M.S. Whittingham, *Chem Rev*. 104 (2004), 4271.
24. W. Chen, L. Mai, Y. Qi and Y. Dai, *J Phys Chem Solids*. 67 (2006), 896.
25. N.A. Chernova, M. Roppolo, A.C. Dillon and M.S. Whittingham, *J Mater Chem*. 19 (2009), 2526.
26. H. Shirakawa, E.J. Louis, A.G. MacDiarmid, C.K. Chiang and A.J. Heeger, *J Chem Soc Chem Commun* (1977), 578.
27. P. Novák, K. Müller, K.S.V. Santhanam and O. Haas, *Chem Rev*. 97 (1997), 207.
28. G. Li, C. Zhang, H. Peng and K. Chen, *Macromol Rapid Commun*. 30 (2009), 1841.
29. X. Lu, Q. Zhao, X. Liu, D. Wang, W. Zhang, C. Wang and Y. Wei, *Macromol Rapid Commun*. 27 (2006), 430.
30. R. Liu and S.B. Lee, *J Am Chem Soc*. 130 (2008), 2942.
31. X. Li, J. Liu and Y. Li, *Appl Phys Lett*. 81 (2002), 4832.
32. L. Fang, Y. Shu, A. Wang and T. Zhang, *J Phys Chem C*. 111 (2007), 2401.
33. S.H. Lee, Y.H. Kim, R. Deshpande, P.A. Parilla, E. Whitney, D.T. Gillaspie, K.M. Jones, A. Mahan, S. Zhang and A.C. Dillon, *Advanced Materials*. 20 (2008), 3627.
34. K.S. Ryu, Y. Lee, K.S. Han and M.G. Kim, *Mater Chem Phys*. 84 (2004), 380.
35. W. Xiao, J.S. Chen, Q. Lu and X.W. Lou, *J Phys Chem C.* 114 (2010), 12048.
36. L. Mai, B. Hu, Y. Qi, Y. Dai and W. Chen, *Int J Electrochem Sci*. 3 (2008), 216